Data-Driven Decentralized Model-Free Predictive Control Microgrid Active Restoration Methods

Tengfei Wei, Xuefeng Zhang, Lixin Wang

***Abstract*—Aiming to address the issue of bus voltage frequency fluctuations caused by unbalanced nonlinear load networking in AC microgrids, this study explores a decentralized data-driven control method based on an improved model-free adaptive predictive control (MF-APC) approach. The dynamic linearization method is employed to linearize the unbalanced nonlinear characteristics of the microgrid at its dynamic operating point, enabling the establishment of a data-driven model that incorporates real-time data. The optimal dynamic linearization parameters are calculated using an enhanced least squares method.**

To enhance the controller's dynamic performance, the historical input and output data of the interface inverter are integrated into the MF-APC model's cost function. Simulation results demonstrate that, compared to the conventional PID-based secondary control method, this approach more effectively suppresses bus voltage frequency fluctuations and achieves the desired control objectives.

***Index Terms*—islanded microgrids, decentralized control, model-free predictive control, data-driven**

I. Introduction

With the continuous progress and rapid development of the global economy, electricity demand and primary energy consumption have both risen, leading to environmental pollution and other associated issues [1]. New green energy technologies, such as wind and solar power, play a crucial role in promoting low-carbon solutions and addressing environmental challenges. During the low-carbon energy transition, AC Micro-Grids (AC-MGs) composed of Distributed Generation (DG) have accelerated the development of new energy-based power systems[1]-[2]. However, during the islanded operation of AC-MGs, self-organized networks of various load types can degrade bus voltage and frequency performance, potentially triggering the operation of distribution network relay protection devices. Specifically, the self-assembled networks of three-phase asymmetrical and nonlinear loads can cause voltage imbalances in the microgrid bus and impair voltage transient performance. Additionally, the nonlinear impedance characteristics of such loads can introduce voltage harmonics, distorting the bus voltage waveform.When an islanded microgrid disconnects due to fault conditions, active restoration techniques enable it to quickly restore critical loads and resume energy supply [3].

Transient shocks during the self-organization of nonlinear asymmetric loads can result in bus voltage imbalances and frequency fluctuations, potentially causing active recovery failures in AC Micro-Grids (AC-MGs). Studies in the microgrids, this study exploresliterature have explored various approaches to address these challenges:

1. Model Predictive Control: Research [4]-[5] investigates the coordination of power and frequency stable responses in generation systems with uneven Distributed Generation (DG) output. While effective, this method requires frequent switching of circuit breakers, which is detrimental to system operation.
2. Variable Slope Sag Control: Another study examines voltage and frequency fluctuations caused by microgrid black starts using thermal units. However, the system analyzed does not account for load self-organizing networks [6].
3. Double Closed-Loop Control Strategy with Feed-Forward Compensation: This strategy successfully smooths voltage and frequency fluctuations caused by load self-organizing networks but does not consider asymmetrical loads[7].
4. Pruning Algorithm for Multi-Objective Black-Start Schemes: Literature [8] explores black-start schemes for distribution networks under voltage and frequency stability constraints. The pruning algorithm addresses the limitations of traditional heuristic optimization methods but does not specifically address load asymmetry.

In practice, the self-organization of a large number of single-phase and nonlinear loads causes the overall network loads to exhibit nonlinear unbalanced characteristics. This leads to negative sequence voltage drops and introduces harmonics, exacerbating operational challenges in AC-MGs.

To address voltage unbalance caused by negative sequence voltage drops, compensation values are often superimposed into control systems. However, their injection into double closed-loop control systems can destabilize system operation [9]-[10]. Studies using sliding mode control with voltage compensation have investigated input current control for matrix converters under grid unbalance, but such systems

Manuscript received November 1, 2024; revised February 11, 2025.

TengFei Wei is an associate professor in School of Electrical Engineering and Information Engineering, Lanzhou University of Technology, Gansu Province, CO 730000 China. (phone:86-1521402724; e-mail: tfwei@lut.eud.cn).

XueFeng Zhang is a postgraduate student of Electrical Engineering and Information Engineering, Lanzhou University of Technology, Gansu Province, CO 730000 China. (e-mail: 1226738059@qq.com).

LiXin Wang is a postgraduate student of Electrical Engineering and Information Engineering, Lanzhou University of Technology, Gansu Province, CO 730000 China. (e-mail: 2312628229@qq.com).

often experience jitter [11]. Similarly, frequency sextupling repetitive control has been applied to mitigate output voltage distortion under nonlinear load conditions, though it requires high modeling accuracy [12].

Fuzzy logic control has been explored to tackle voltage disturbances during grid-connected/off-grid switching processes, but it heavily relies on expert experience [13]. Optimization strategies for microgrid fault recovery have also been proposed to balance multiple objectives, achieving efficient and cost-effective recovery in real-world applications [14]. Deep learning algorithms have enabled self-healing mechanisms for automatic fault detection and recovery in microgrids [15], while distributed energy management systems have been utilized to coordinate solar, wind, and battery storage for stable power restoration after grid failures [16].

Real-time data analysis using IoT technology has further advanced fault detection and recovery. By deploying sensors and intelligent devices, microgrid operation data can be collected in real time, enabling fault localization and recovery planning through big data analysis [17]. Communication-assisted collaborative restoration methods have also been introduced, leveraging efficient communication networks to coordinate multiple microgrid units and enhance recovery efficiency [18]. Fault-tolerant control strategies incorporating advanced power electronics and intelligent algorithms allow islanded microgrids to independently restore power and maintain stability when disconnected from the main grid [19].

Most of the above studies focus on controller design when the AC Micro-Grid (AC-MG) structure is well understood, and accurate models are available. However, if the model cannot adequately represent the AC-MG's structure or parameter variations, the control performance falls short of expectations. Addressing the challenge of reducing a controller's dependence on the microgrid model when dealing with self-assembled load networks remains an unresolved issue.

MF-AC enables the control of discrete-time nonlinear systems using operational data, eliminating the need for an accurate system model [20]. Model-Free Adaptive Predictive Control (MF-APC) builds on MF-AC by computing the dynamic linearization parameters at future time steps, enabling optimal output prediction [21]-[22]. For instance, MF-APC combined with a sliding mode observer has been used to suppress output current ripple, though selecting key parameters within the MF-APC framework remains challenging [23]. Additionally, MF-APC has been employed to address zero-sequence loop current issues in shunt converters [24].

This paper addresses the power quality issues caused by nonlinear asymmetric loads and the challenges in selecting parameters for the MF-APC controller during the active recovery process of islanded AC microgrids (AC-MG). Building on MF-APC, it proposes a Data Reconstruction Model-Free Adaptive Predictive Control (DR-MF-APC) method to establish a data-driven decentralized control strategy for AC-MG.

The DR-MF-APC method utilizes AC-MG bus power operation data to design a dynamic linearization function, transforming the transient disturbance suppression problem during active recovery into an iterative optimization of the cost function. This data-driven decentralized controller transfers real-time optimal power reference values to droop control based on load power demands, effectively suppressing voltage and frequency fluctuations by adjusting the distributed generation (DG) output power. Compared to traditional MF-APC data-driven strategies, the proposed DR-MF-APC method is less sensitive to key parameter selection, mitigating the risk of voltage and frequency offsets caused by variations in DG output power. Additionally, the effectiveness of the proposed control strategy in managing the impact of load self-organized networks and variations in control parameters is verified through a designed example.

II. Dynamic Linearization of Microgrids Models

The block diagram of the power generation unit in AC-MG is shown in Fig. 1. It consists of power droop control and a double closed-loop control for voltage and current. The power control of the generation unit relies on the measured voltage u_{abc} and current i_{abc} at the DGi access point. Using these measurements, the active and reactive power $P_i^{\mathrm{vsc}}(k)$ and $Q_i^{\mathrm{vsc}}(k)$ outputs of DGi are calculated.

The reference values for active (P_i^*) and reactive power (Q_i^*) are provided, and the power droop control mechanism stabilizes the output power of the generation unit based on these reference values.

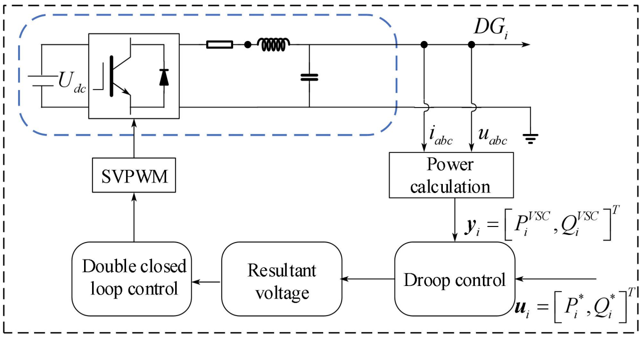

Fig. 1. Power control block diagram of DGi power generation unit

For the microgrid system depicted in Fig. 1, which includes n distributed generation units, the dynamic behavior of the i-th distributed generation unit DGi is influenced by the nonlinear load and other coupling characteristics within the microgrid. Considering these factors, the dynamic nonlinear discrete mathematical model for DGi, which spans from droop control to the point of common coupling (PCC), represents the relationship between the input and output power as follows:

$$\begin{cases} P_i^{\mathrm{vsc}}(k+1)=f_{\mathrm{p}}(P_i^{\mathrm{vsc}}(k),\cdots,P_i^{\mathrm{vsc}}(k-n_{\mathrm{v}}), \\ \qquad \cdots,P_i^*(k),\cdots,P_i^*(k-n_{\mathrm{u}})) \\ Q_i^{\mathrm{vsc}}(k+1)=f_{\mathrm{g}}(Q_i^{\mathrm{vsc}}(k),\cdots,Q_i^{\mathrm{vsc}}(k-n_{\mathrm{v}}), \\ \qquad \cdots,Q_i^*(k),\cdots,Q_i^*(k-n_{\mathrm{u}})) \end{cases} \tag{1}$$

In the formula, $P_i^{\mathrm{vsc}}(k+1)$ and $Q_i^{\mathrm{vsc}}(k+1)$ represent the predicted active and reactive power outputs of the system at a future time ; f_p and f_g are unknown nonlinear vector-valued functions describing the active and reactive power dynamics, respectively. The parameters n_v and n_u denote the output and input orders of the microgrid system, representing the number of past data points required to predict the power at time $k+1$. These are typically positive integers. $P_i^{\mathrm{vsc}}(k-n_{\mathrm{v}})$ is the system's active power output at time $k-n_{\mathrm{v}}$ under the influence of order n_{v}, and $P_i^{\mathrm{vsc}}(k-n_u)$ is the reference value of the optimal active power determined by the droop control mechanism at time $k-n_u$ under the order of n_u.

AC-MG is a system containing several controllers with the same structure so that the output power measurement value of DGi is $\boldsymbol{y}_i=\left[P_i^{\mathrm{vsc}},Q_i^{\mathrm{vsc}}\right]^T$ and the set power during microgrid scheduling is $\boldsymbol{u}_i=\left[P_i^*,Q_i^*\right]^T$, then Equation (2) can be uniformly expressed as:

$$\begin{aligned}\boldsymbol{y}_i(k+1)=f(&\boldsymbol{y}_i(k),\cdots,\boldsymbol{y}_i(k-n_{\mathrm{v}}),\\&\cdots,\boldsymbol{u}_i(k),\cdots,\boldsymbol{u}_i(k-n_{\mathrm{u}}))\end{aligned} \tag{2}$$

Where $\boldsymbol{y}_i(k+1)$ is the system output prediction value, which is to be determined by the system input and output data through the subsequent dynamic linearization method; f is an unknown nonlinear function used to link the system data; $\boldsymbol{y}_i(k-n_{\mathrm{v}})$ is the system output data of $k-n_{\mathrm{v}}$ at the historical moment, specifically the power measurement; and $\boldsymbol{u}_i(k-n_{\mathrm{u}})$ is the optimal control input data of the system at the historical moment of $k-n_{\mathrm{u}}$, i.e., the optimal reference value derived from the droop control.

III. Improved Model-Free Adaptive Predictive Controller Design

As the power generation unit DGi is in operation, to stabilize the bus voltage and frequency of AC-MG, its output power $\boldsymbol{y}_i$ is continuously adjusted by the reference power $\boldsymbol{u}_i$. Therefore, under the actual operation of the power generation unit, the reference power $\boldsymbol{u}_i(k)$ is continuously changes, and the amount of change is bounded. As a result, the partial derivative of the reference power $\boldsymbol{u}_i(k)$ exists and is continuous. The dynamic linearization of Equation (2) requires the satisfaction of two theorems[25], and when $\left|\Delta u_i(k)\right|\neq 0$ is satisfied, a bounded Pseudo Jacobian Matrix $\boldsymbol{\Phi}_i(k)$ (PJM) can be determined. This matrix allows the system described by Equation (2) to be equivalently transformed into an incremental difference equation of the following form:

$$\boldsymbol{y}_i(k+1)=\boldsymbol{y}_i(k)+\boldsymbol{\Phi}_i(k)\left(\boldsymbol{u}_i(k)-\boldsymbol{u}_i(k-1)\right) \tag{3}$$

The element $\phi_{ii}(k)$ in the matrix $\boldsymbol{\Phi}_i(k)$ changes dynamically with moment k, representing the vector value of the gradient vector of f about $\boldsymbol{u}_i$ at a point between $\boldsymbol{u}_i(k-1)$ and $\boldsymbol{u}_i(k)$. $\phi_{ii}(k)$. This element is referred to as the bounded time-varying Pseudo Partial Derivative (PPD). The method for obtaining the PPD will be discussed in more detail in subsection 4. Equation (3) represents the dynamic linearization model for islanded microgrids, which is used in the design of a data-driven decentralized model-free predictive control strategy for microgrid active restoration. Notably the PPD is purely a mathematical concept and does not have a direct physical interpretation. However, the existence of the PPD can be proven through mathematical derivation. The value of PJM composed of the PPD, reflects the strength of the coupling relationship between the input and output quantities of the system.

The data-driven decentralized model-free predictive control strategy operates by adjusting the system output power for the next time step. This is done by modifying the difference between the current input power $\boldsymbol{u}_i(k)$ at the current moment and the input power, which in turn influences the DGi output power.

Let the control output increment vector be:

$$\Delta\boldsymbol{u}_i(k)=\boldsymbol{u}_i(k)-\boldsymbol{u}_i(k-1) \tag{4}$$

Then Equation (3) can be written in the form of a one-step output prediction equation:

$$\boldsymbol{y}_i(k+1)=\boldsymbol{y}_i(k)+\boldsymbol{\Phi}_i(k)\Delta\boldsymbol{u}_i(k) \tag{5}$$

In the actual system operation process, the predicted output value for one step within the control time domain is not necessarily the optimal control output. To predict the optimal output of the AC-MG system within the prediction time domain, based on Equation (5), the N-step DGi output power prediction value and the control increment column vector are given by Equations (6) and (7):

$$\boldsymbol{Y}_i^{(N)}(k+1)=[\boldsymbol{y}_i(k+1),\cdots,\boldsymbol{y}_i(k+N)]^{\mathrm{T}} \tag{6}$$

$$\Delta\boldsymbol{U}_i^{(N)}(k)=[\Delta\boldsymbol{u}_i(k),\cdots,\Delta\boldsymbol{u}_i(k+N-1)]^{\mathrm{T}} \tag{7}$$

The column vector $\boldsymbol{y}_i(k+N)$ denotes the N-step output power prediction value of DGi at the $k+N$ th moment, and the column vector $\Delta\boldsymbol{u}_i(k+N-1)$ is the N-step input power prediction value of DGi at the $k+N-1$th moment. A larger value of N can capture more dynamic characteristics of the AC-MG system, but it also increases the computational load. Typically, N is chosen between 3 and 10 [26]. Equation (5) can be expanded into an N-step output prediction equation as follows:

$$\boldsymbol{Y}_i^{(N)}(k+1)=\boldsymbol{E}\cdot\boldsymbol{y}_i(k)+\boldsymbol{H}(k)\Delta\boldsymbol{U}_i^{(N)}(k) \tag{8}$$

Where $\boldsymbol{E}$ is the unit-column vector of $N\times 1$; $\boldsymbol{H}(k)$ is the square matrix of $N\times N$, the elements of which consist of the

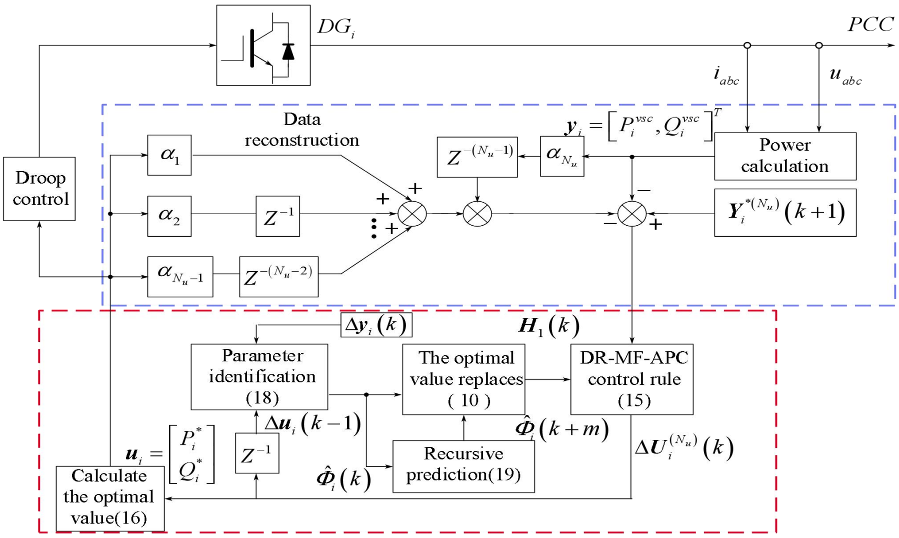

Fig. 2. Block diagram of DR-MF-APC structure

PJM matrices $\boldsymbol{\Phi}_i$ at different moments, and $\boldsymbol{Y}_i^{(N)}(k+1)$ can be given by the computation of $\boldsymbol{\Phi}_i$. Where $\boldsymbol{H}(k)$ is represented as follows:

$$\boldsymbol{H}(k)=\begin{pmatrix} \boldsymbol{\Phi}_i(k) & 0 & 0 & 0 & \cdots & 0 \\ \boldsymbol{\Phi}_i(k) & \boldsymbol{\Phi}_i(k+1) & 0 & 0 & \cdots & 0 \\ \vdots & \vdots & \ddots & \vdots & & \vdots \\ \boldsymbol{\Phi}_i(k) & \cdots & & \boldsymbol{\Phi}_i(k+N_u-1) & & \\ \vdots & & & \vdots & \ddots & 0 \\ \boldsymbol{\Phi}_i(k) & \boldsymbol{\Phi}_i(k+1) & \cdots & \boldsymbol{\Phi}_i(k+N_u-1) & \cdots & \boldsymbol{\Phi}_i(k+N-1) \end{pmatrix}_{N\times N} \tag{9}$$

Equation (8) incorporates all the predicted values over the prediction time domain, but not all predicted values are required during the controller's operation. To reduce the computation needed for the control increment $\Delta\boldsymbol{U}_i^{(N)}(k)$ of the DR-MF-APC active recovery strategy, the model focuses on a subset of the predicted values.

Notably the data-driven method designed using neural networks relies on historical data for training and making predictions. However, if the system encounters situations that have not occurred in the historical dataset, the model may generate inaccurate predictions or unexpected behavior. The data-driven approach proposed in this paper overcomes this limitation by using online measurement data for predictions.

To simplify the representation of N_u (the prediction step), it refers to the number of historical data points and the predictive time length. In practice, the value of N_u lies within the range of $2 \le N_u \le 7$ [25], without requiring a large amount of data.

When the moment $k > N_u$, the system tracking error tends to be within a reasonable range; if $\Delta\boldsymbol{u}_i(k+j-1)=0$, then $\boldsymbol{H}(k)$ can be simplified to $\boldsymbol{H}_1(k)$, which is expressed as follows:

$$\boldsymbol{H}_1(k)=\begin{pmatrix} \boldsymbol{\Phi}_i(k) & 0 & 0 & 0 \\ \boldsymbol{\Phi}_i(k) & \boldsymbol{\Phi}_i(k+1) & 0 & 0 \\ \vdots & \vdots & \ddots & \vdots \\ \boldsymbol{\Phi}_i(k) & \boldsymbol{\Phi}_i(k+1) & \cdots & \boldsymbol{\Phi}_i(k+N_u-1) \\ \vdots & \vdots & \cdots & \vdots \\ \boldsymbol{\Phi}_i(k) & \boldsymbol{\Phi}_i(k+1) & \cdots & \boldsymbol{\Phi}_i(k+N_u-1) \end{pmatrix}_{N\times N_u} \tag{10}$$

In Equation (8), the optimal output power of the system at the time $k+1$ is denoted as $\boldsymbol{Y}_i^{(N_u)}(k+1)$. When the step size is N_u , the predicted value of the optimal input to sag power of the system at the time of k is $\Delta\boldsymbol{U}_i^{(N_u)}$, and $\Delta\boldsymbol{U}_i^{(N_u)}$ is expressed as follows:

$$\begin{aligned} \Delta\boldsymbol{U}_i^{(N_u)}(k) &= \boldsymbol{U}_i^{(N_u)}(k)-\boldsymbol{U}_i^{(N_u)}(k-1) \\ &= [\Delta\boldsymbol{u}_i(k),\cdots,\Delta\boldsymbol{u}_i(k+N_u-1)]^{\mathrm{T}} \end{aligned} \tag{11}$$

Then the N-step output prediction Equation (8) can be rewritten as:

$$\boldsymbol{Y}_i^{(N_u)}(k+1)=\boldsymbol{E}\cdot\boldsymbol{y}(k)+\boldsymbol{H}_1(k)\Delta\boldsymbol{U}_i^{(N_u)}(k) \tag{12}$$

Equation (12) represents the dynamic linearization model of the DGi within the DR-MF-APC active recovery strategy. This strategy predicts the output power of DG $\Delta\boldsymbol{u}_i(k)$ in the next moment based on the reference power increment of the DGi at the current moment through Equation (12) Predicting the output power of DGi at the next moment $\boldsymbol{y}_i(k+1)$.

The DR-MF-APC active recovery strategy consists of three main components: parameter identification, recursive prediction, and data reconstruction, as depicted in Fig. 2.

The pseudo-Jacobian matrix $\boldsymbol{\Phi}_i(k)$,which cannot be obtained directly, requires the parameter identification part to estimate the optimal value of $\boldsymbol{\Phi}_i(k)$ online and use $\hat{\boldsymbol{\Phi}}_i(k)$ instead of $\boldsymbol{\Phi}_i(k)$ for subsequent computation. Additionally, the rest of the PJM matrix $\boldsymbol{\Phi}_i(k+1),\ldots,\boldsymbol{\Phi}_i(k+N_u-1)$ in $\boldsymbol{H}_1(k)$ needs data from future moments to calculate its optimal estimate $\hat{\boldsymbol{\Phi}}_i(k+m)$, where $m > 0$. Based on the parameter identification part, we obtain the existing estimate $\hat{\boldsymbol{\Phi}}_i(1),\ldots,\hat{\boldsymbol{\Phi}}_i(k)$, and then make the recursive prediction of $\hat{\boldsymbol{\Phi}}_i(k+m)$ through autoregressive method. Through the two parts of parameter identification and recursive prediction to obtain the pseudo-Arkobi matrix

$\boldsymbol{\Phi}_i(k)$ all the optimal estimates of $\hat{\boldsymbol{\Phi}}_i(k+1),...,\hat{\boldsymbol{\Phi}}_i(k+N_{\mathrm{u}}-1)$,and finally by the prediction model of power generation units (12) and $\Delta\boldsymbol{U}_i^{(N_{\mathrm{u}})}(k)$, its output power prediction value $\boldsymbol{Y}_i^{(N_{\mathrm{u}})}(k+1)$ can be calculated.

The transient process of the load self-organizing network in the AC-MG impacts the DGi output power, and to manage this, the DR-MF-APC strategy provides corresponding reference power compensation. This compensation helps to suppress the jitter in the DGi power within the load self-organizing network, ensuring smoother system operation.

To achieve this, the strategy weights and integrates the historical optimal prediction values and the system output data collected at the current moment. The integration of these two data sources forms the input data for the decentralized controller $\boldsymbol{Y}_i^{(N_{\mathrm{u}})}(k+1)$. By adjusting the proportion of the historical optimal prediction value and the measured value.

Considering the above, the following objective function is proposed for $\Delta\boldsymbol{U}_i^{(N_{\mathrm{u}})}(k)$:

$$J\left(\Delta\boldsymbol{U}_i^{(N_{\mathrm{u}})}(k)\right)=\left(\boldsymbol{M}_i^{(N_{\mathrm{u}})}(k+1)\right)^{\mathrm{T}}\boldsymbol{M}_i^{(N_{\mathrm{u}})}(k+1) + \lambda\left(\Delta\boldsymbol{U}_i^{(N_{\mathrm{u}})}(k)\right)^{\mathrm{T}}\Delta\boldsymbol{U}_i^{(N_{\mathrm{u}})}(k) \tag{13}$$

In the formula, $\boldsymbol{M}_i^{(N_{\mathrm{u}})}(k+1)$ the system output error control term, denoted as $\boldsymbol{M}_i^{(N_{\mathrm{u}})}(k+1)$, is used to limit the inverter output so that its output power remains constantly close to the reference value $\Delta\boldsymbol{U}_i^{(N_{\mathrm{u}})}(k)$. The term $\Delta\boldsymbol{U}_i^{(N_{\mathrm{u}})}(k)$ represents the incremental vector of control inputs to be taken; z^{-n} is the delay of the system operation data, where $n\in[0,N_u-1]$, $\boldsymbol{E}$ is the unit column vector of N_u-1 ; the weight factor λ is the only parameter that is adjusted online, determining the weight of the $\Delta\boldsymbol{U}_i^{(N_{\mathrm{u}})}(k)$ output error term $\Delta\boldsymbol{U}_i^{(N_{\mathrm{u}})}(k)$ in the criterion function, and is generally taken as $\lambda>0$ [27].

$\boldsymbol{M}_i^{(N_{\mathrm{u}})}(k+1)$ in Equation (13) denotes the following:

$$\boldsymbol{M}_i^{(N_{\mathrm{u}})}(k+1)=\boldsymbol{Y}_i^{*(N_{\mathrm{u}})}(k+1)-[\sum_{j=2}^{N_{\mathrm{u}}}\alpha_{j-1}\boldsymbol{u}_i(k-N_{\mathrm{u}}+2) + \alpha_{N_{\mathrm{u}}}\boldsymbol{y}_i(k-N_{\mathrm{u}}+1)]\tilde{\boldsymbol{E}}-\boldsymbol{Y}_i^{(N_{\mathrm{u}})}(k+1) \tag{14}$$

Where $\boldsymbol{Y}_i^{*(N_{\mathrm{u}})}(k+1)$ in Equation (12) represents the desired output matrix of N_u step, and each element $y^*(k+1)$ corresponds to the reference values of active and reactive power $k+1$. These reference values are determined according to the microgrid's scheduling information[28]. $\alpha_{N_{\mathrm{u}}}$ is the reconstruction data weighting coefficient. It helps prevent system instability caused by sudden changes in control increments and addresses the load self-organization problem. The weighting coefficient ensures that the system stabilizes by adjusting the control increments while achieving the precise tracking control target; $\tilde{\boldsymbol{E}}$ represents the unit column vector of $N_{\mathrm{u}}\times 1$.

The goal of this strategy is to suppress jitter in the output power values generated by the active recovery strategy, which can occur due to variations in the load caused by the self-organizing DGis.

To address this, a reconstructed dataset is formed by combining the DGi historical data ($k-N_{\mathrm{u}}+1$) and time-measurement data ($\boldsymbol{y}_i(k-N_{\mathrm{u}}+1)$), and the controller's historical optimal output prediction $\boldsymbol{u}_i(k-N_{\mathrm{u}}+2)$ is used to reconstruct the objective function.

By combining Equations (12) and (13) to the extremes, the designed DR-MF-APC control law can be obtained as follows:

$$\begin{aligned}\Delta\boldsymbol{U}_i^{(N_{\mathrm{u}})}(k)&=[\boldsymbol{H}_1^{\mathrm{T}}(k)\boldsymbol{H}_1(\mathrm{k})+\lambda\tilde{\boldsymbol{E}}]^{-1}\boldsymbol{H}_1^{\mathrm{T}}(k)\\&\times[\boldsymbol{Y}_i^{*(N_{\mathrm{u}})}(k+1)-\tilde{\boldsymbol{E}}(\sum_{j=2}^{N_{\mathrm{u}}}\alpha_{j-1}\boldsymbol{u}_i(k-N_{\mathrm{u}}+2)\\&+\alpha_{N_{\mathrm{u}}}\boldsymbol{y}_i(k-N_{\mathrm{u}}+1)+\boldsymbol{y}_i(k+1))]\end{aligned} \tag{15}$$

Therefore, the optimal input reference power in DGi droop control at the current moment can be expressed as:

$$\boldsymbol{u}_i(k)=\boldsymbol{u}_i(k-1)+\boldsymbol{g}^T\Delta\boldsymbol{U}_i^{(N_u)}(k)=\left[\boldsymbol{P}_i^*(k),\boldsymbol{Q}_i^*(k)\right]^T \tag{16}$$

Where $g=[1,0,...,0]_{Nu\times 1}^T$ is the coefficient multiplied to obtain the optimal input prediction at the current moment.

IV. Recursive Gradient Estimation Algorithm for Parameters of Output Prediction Equations

In the incremental nonlinear dynamic difference equation of the power generation unit DGi, all the possible nonlinear time-varying parameters of the AC-MG and perturbations, such as changes in the AC-MG architecture, will affect the output power of the DGi. All the above effects are reflected in the time-varying PJM $\boldsymbol{\Phi}_i(k)$, so the dynamic characteristics of $\boldsymbol{\Phi}_i(k)$ the system will become very complicated. To obtain the PJM, and considering the slow time-varying values of PPD in the PJM $\boldsymbol{\Phi}_i(k)$, the parameters are identified using the projection algorithm, and the objective function of the projection algorithm is as follows:

$$J\left(\boldsymbol{\Phi}_i(k)\right)=\left\|\Delta\boldsymbol{y}_i(k)-\boldsymbol{\Phi}_i(k)\Delta\boldsymbol{u}_i(k-1)\right\|^2 + \mu\left\|\boldsymbol{\Phi}_i(k)-\hat{\boldsymbol{\Phi}}_i(k-1)\right\|^2 \tag{17}$$

In the formula, $\Delta\boldsymbol{y}_i(k)$ represents the difference between the system's output data at time k and at time $k-1$; , while $\Delta\boldsymbol{u}_i(k-1)$ denotes the difference between the system's input data at the time $k-1$ and the input data of the system at the time $k-2$; $\hat{\boldsymbol{\Phi}}_i(k)$ is the optimal estimate of the value of. By calculating $\hat{\boldsymbol{\Phi}}_i(k)$, we can substitute the

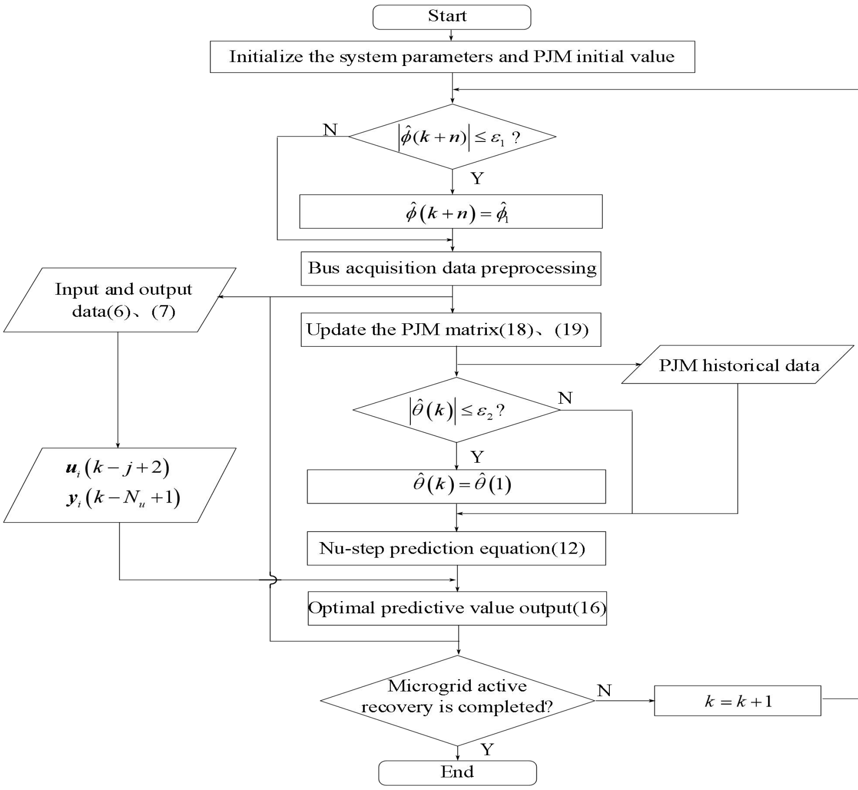

Fig. 3. Flowchart of active recovery based on DR-MF-APC

element $\boldsymbol{\Phi}_i(k)$ in $\boldsymbol{H}_1(k)$ with the optimal estimation value. The smaller the penalty factor μ, the faster $\boldsymbol{\Phi}_i(k)$ can respond to the DGi situation of the generating unit. However, a smaller value may lead to increased data jitter of $\boldsymbol{\Phi}_i(k)$, so it is generally chosen as $\mu>0$ [23].

To find the extreme values of Equation (17), we can express $\hat{\boldsymbol{\Phi}}_i(k)$ as follows:

$$\hat{\boldsymbol{\Phi}}_i(k)=\hat{\boldsymbol{\Phi}}_i(k-1)+\frac{\eta\Delta\boldsymbol{u}_i(k-1)}{\mu+\|\Delta\boldsymbol{u}_i(k-1)\|^2} \times[\Delta\boldsymbol{y}_i(k)-\hat{\boldsymbol{\Phi}}_i(k-1)\Delta\boldsymbol{u}_i(k-1)] \tag{18}$$

where the step factor η enables $\hat{\boldsymbol{\Phi}}_i(k)$ to converge faster to $\boldsymbol{\Phi}_i(k)$; however, larger η values may cause the parameter identification algorithm to not converge, usually $\eta\in(0,2]$ [23] $\boldsymbol{H}_1(k)$ in $\boldsymbol{\Phi}_i(k+1),...,\boldsymbol{\Phi}_i(k+m),...,\boldsymbol{\Phi}_i(k+N_u-1)$ cannot be obtained directly from the current run data, it needs to be estimated using the optimal estimate $\hat{\boldsymbol{\Phi}}_i(1),...,\hat{\boldsymbol{\Phi}}_i(k)$, to calculate $\boldsymbol{H}_1(k)$.

The autoregressive forecasting model with the best estimate $\hat{\boldsymbol{\Phi}}_i(1),...,\hat{\boldsymbol{\Phi}}_i(k)$ is expressed as follows:

$$\hat{\boldsymbol{\Phi}}_i(k+m)=\sum_{a=1}^{n_p}\theta_a(k)\hat{\boldsymbol{\Phi}}_i(k+m-a) \tag{19}$$

Where $\theta_a(k)$ is the recursive forecast coefficient, similar to $\boldsymbol{\Phi}_i(k)$, which can be obtained by projection algorithm, and n_p is the autoregressive order, which can take values from 2 to 7[23].

Let $\boldsymbol{B}(k)=\left[\theta_1(k),\cdots,\theta_{n_p}(k)\right]^T$, then the optimal estimate of the recursive forecast coefficient $\hat{\boldsymbol{B}}(k)$ can be expressed as:

$$\hat{\boldsymbol{B}}(k)=\hat{\boldsymbol{B}}(k-1)+\frac{\hat{\boldsymbol{\Phi}}_i(k-1)}{\delta+\|\hat{\boldsymbol{\Phi}}_i(k-1)\|^2} \times[\hat{\boldsymbol{\Phi}}_i(k)-\hat{\boldsymbol{\Phi}}_i^T(k-1)\hat{\boldsymbol{\theta}}(k-1)] \tag{20}$$

Here, δ is the scaling factor. Selecting an appropriate scaling factor can enhance the accuracy of the estimated value, which is typically set to $\delta(0,1]$ [23].

When the estimated value $\hat{\phi}(k)$ of the element $\phi(k)$ in $\boldsymbol{\Phi}_i(k)$ and the estimated value $\hat{\boldsymbol{\theta}}_{n_p}(k)$ of the recursive forecast coefficients do not converge to either 0 or ∞, then the system described by Equation (2) is output-controllable at the specified feasible set-point. To improve the algorithm's ability to track time-varying parameters, a reset algorithm can be designed. This algorithm is activated when $\hat{\phi}(k)$ and $\hat{\boldsymbol{\theta}}_{n_p}(k)$ are smaller than the normal number thresholds $\varepsilon_1,\varepsilon_2$:

$$\begin{aligned}&\hat{\phi}(k+n)=\hat{\phi}(1)>0,(|\hat{\phi}(k+n)|\le\varepsilon_1),\\&n\in[0,N_u-1],\hat{\theta}(k)=\hat{\theta}(1)>0,\\&(|\hat{\theta}(k)|\le\varepsilon_2)\end{aligned} \tag{21}$$

Where $\hat{\phi}(1)$ is the initial value of $\hat{\phi}(k)$ and the threshold value in this paper is $\varepsilon_1 = \varepsilon_2 = \varepsilon = 10^{-4}$.

The micro-grid active restoration algorithm based on DR-MF-APC needs to input initial parameters, variables, algorithm stop criteria, and output the optimal solution. The flow chart is shown in Fig.3.

DR-MF-APC is a data-driven control method. Once the algorithm's initial values and parameters are initialized, the input and output data required by the algorithm are used in the dynamic linearization process. To perform the dynamic linearization of Equation (12) for each data set, it is necessary to identify the current time parameters $\boldsymbol{\Phi}_i(k)$ and future time parameters $\hat{\boldsymbol{\Phi}}_i(k+m)$ in the PJM parameters $\boldsymbol{H}_1(k)$. Among them, $\hat{\boldsymbol{\Phi}}_i(k+m)$ cannot be calculated directly and must be estimated using a low-order prediction method.

Each data set involved in the dynamic linearization process includes portions of data from both the current and historical times. The dynamic linearization equation then provides the optimal control law, which is used to determine the optimal solution. After calculating the optimal output solution for each step, the algorithm re-evaluates its ability to track time-varying parameters and determines whether a reset is required.

V. Simulation Experiments and Comparative Analysis of Results

A. Simulation Parameter

Nonlinear asymmetrical loads and load self-organization can simultaneously cause fluctuations in bus voltage and frequency. Simulation experiments will compare the PID negative sequence compensation recovery strategy(NSCs)[28] with the DR-MF-APC active recovery strategy, followed by an analysis of the simulation results. The structural diagram of the simulation experiment system is shown in Fig.4 (L denotes the load).

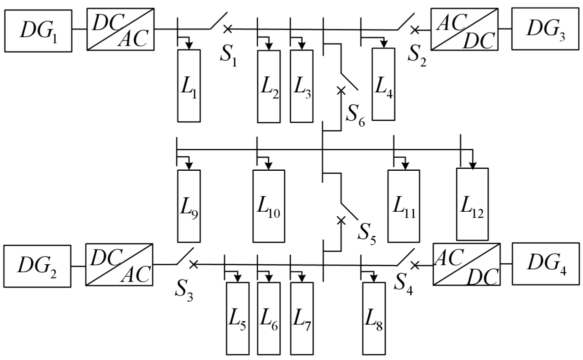

Fig. 4. Silo AC-MG active recovery architecture

The AC-MG system consists of four generating units: DG1, DG2, DG3, and DG4. The rated output voltage and frequency of each DGi are 380V and 50Hz, respectively. All four DGs in the AC-MG system employ the decentralized DR-MF-APC active recovery strategy, with the weighting factor λ is set to 8.6.

Load 1 is classified as a first-level load; loads 2–7 and 10 are second-level loads; and loads 8–9 and 11–12 are third-level loads. Among these, loads 3 and 9 are asymmetrical loads, while load 11 is a nonlinear load, simulated using a three-phase uncontrolled rectifier circuit. The simulation parameters for DGi, the loads, and other components are provided in Table I.

TABLE I
AC-MG PARAMETERS

Parameters	Numerical value
Primary load (kW/ kvar)	15/10
Secondary load (kW/ kvar)	10/5
Tertiary load (kW/ kvar)	8/6
Filter circuit (μF /mH)	1.4/6.2
Line Impedance (Ω)	0.2+ j0.1e-3
DG_1 /DG_2 (kVA)	40
DG_3 /DG_4 (kVA)	50
Simulation time (ms)	300
Switching frequency (kHz)	10

At the initial moment of the system, only the critical load 1 remains active, while the rest of the island is in a full blackout state. At 0s, DG1 begins active recovery, starting with load 1, closing circuit breaker S1, and establishing the initial voltage and frequency of branch 1. Simultaneously, DG2 starts active recovery at 0s, closing circuit breaker S2 and establishing the initial voltage and frequency of branch 2. At 0.01s, load 5 is added. At 0.02s, loads 2 and 6 are sequentially introduced.

At 0.04s, the first asymmetric load 3 and load 7 are added to branch 1. At 0.06s, loads 4 and 8 are introduced, completing the initialization of the two branches and initiating the system's pre-synchronization control. At 0.08s, circuit breakers S5 and S6 are closed. Between 0.1 and 0.12s, circuit breakers S3 and S4 are closed, bringing DG3 and DG4 online. At 0.16s, secondary load 10 is introduced, followed by the second asymmetric load at 0.18s. At 0.2s, nonlinear load 11 is added, and finally, load 12 is introduced at 0.22s. The active recovery of the islanded microgrid concludes at 0.3s.

TABLE II
INITIAL OF DIFFERENT CONTROL STRATEGIES

MF-APC	DR-MF-APC
$\hat{\phi}(1)=\hat{\phi}(2)=8.5$, $\hat{\phi}(3)=\hat{\phi}(4)=8.5$, $[\theta(1),\theta(2)]^T=[1.6,0.8]^T$ $\hat{\theta}(3)=0.9$	$\hat{\phi}(1)=\hat{\phi}(2)=8.5$, $\hat{\phi}(3)=\hat{\phi}(4)=8.5$, $[\theta(1),\theta(2)]^T=[1.6,0.8]^T$ $\hat{\theta}(3)=0.9$ $a_{N_u}=[11.6,46.5,29.5,45]^T$

TABLE III
INITIAL OF DIFFERENT CONTROL STRATEGIES

NSCs	MF-APC	DR-MF-APC
$K_{UP}=300$	$\mu=0.02,\delta=0.86$,	$\mu=0.02,\delta=0.86$,
$K_{UI}=100$	$\eta=0.71,\varepsilon=10^{-4}$	$\eta=0.71,\varepsilon=10^{-4}$
$K_{IP}=300$	$n_P=3,N=5$,	$n_P=3,N=5$,
$K_{II}=0.1$	$N_B=4,M=4$	$N_B=4,M=4$

Based on the rolling optimization principle, larger prediction steps improve result accuracy but lead to increased computational demands, particularly in fast-response systems. Therefore, selecting an appropriate N_u value is critical. In this study, $N_u=4$. The parameters of the different control strategies are detailed in Tables II and III. Value refers to[23][25][27].

B. Unbalanced nonlinear load commissioning system performance

Figure 5(a) shows that when the negative sequence compensation recovery strategy is used, the bus voltage oscillation amplitude reaches 0.7pu after 0.2s of introducing nonlinear loads, whereas the oscillation amplitude with the DR-MF-APC strategy is reduced to 0.43pu. While the traditional negative sequence compensation recovery strategy can maintain bus voltage stability over a limited period for loads containing single unbalanced elements such as load 3, it fails to stabilize the bus voltage during active recovery when handling multiple unbalanced loads, such as loads 3, 9, and nonlinear load 11. This results in insufficient voltage-frequency dynamic response and significant overshooting during the recovery process.

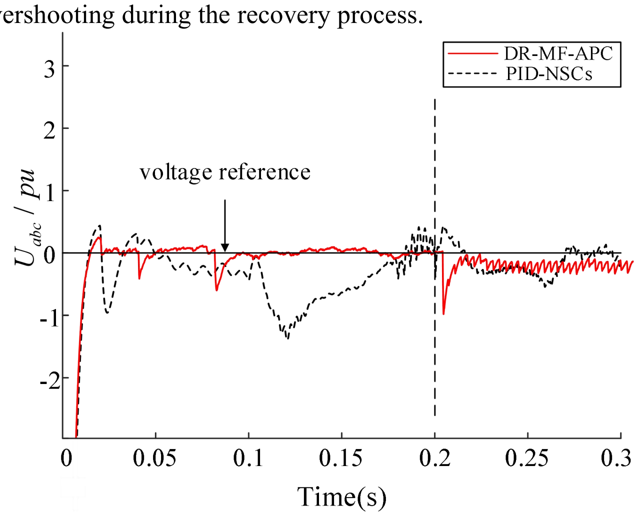

(a)

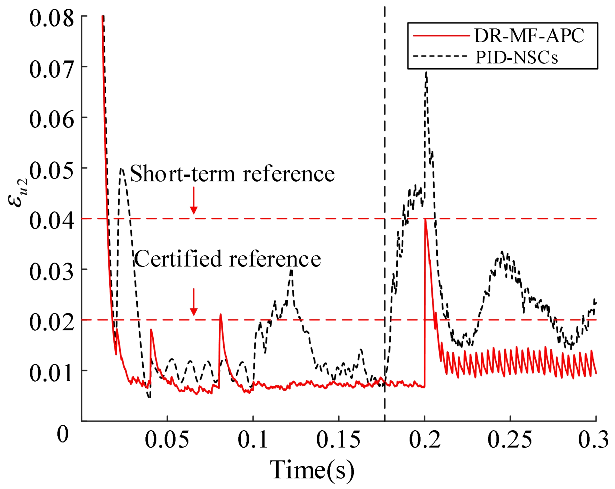

(b)

Fig. 5. System voltage unbalance fluctuation
(a, bus voltage magnitude; b, bus voltage unbalance)

Figure 5(b) illustrates the bus voltage negative sequence unbalance degree. After introducing nonlinear asymmetrical loads at 0.2s, the instantaneous unbalance degree fluctuates sharply, exceeding the short-term reference line and reaching 6.87% during 0.2–0.22s. According to national electric energy standards, the bus voltage unbalance degree should not exceed 2% under normal conditions and 4% for short-term deviations. Using the DR-MF-APC active recovery strategy, the fluctuations in bus voltage and the negative sequence unbalance degree are effectively suppressed, keeping the unbalance degree within the standard and short-term reference limits after the nonlinear asymmetrical load is introduced.

In Figure 6, the upper and lower limits of allowable frequency variation are indicated by $10\cdot\Delta f_{\max}$ and $10\cdot\Delta f_{\min}$. In Fig.5, at 0.08s, 0.1s, and 0.12s, when the DGs are integrated into the system, significant transient frequency fluctuations are observed. Among these, the first asymmetrical load (group 3) operates under the control of a single DG1 inverter, resulting in pronounced system frequency fluctuations. In contrast, the second asymmetrical load (group 9) operates with the simultaneous inverters of DG1 and DG2, leading to comparatively smaller transient frequency fluctuations.

When nonlinear loads self-organize, they cause a sharp frequency drop and frequency jitter after 0.2s. The frequency jitter amplitudes for the negative sequence compensation recovery strategy and the DR-MF-APC active recovery strategy are 1.32 Hz and 0.53 Hz, respectively. This demonstrates that the negative sequence compensation strategy can effectively suppress fluctuations for a single asymmetrical load and multiple machines before 0.1s. However, when managing self-organized networks of multiple asymmetrical loads with DGs, the PID-based negative sequence compensation strategy struggles to suppress transient fluctuations within a short time frame, thereby increasing the risk of secondary power loss for AC-MG loads.

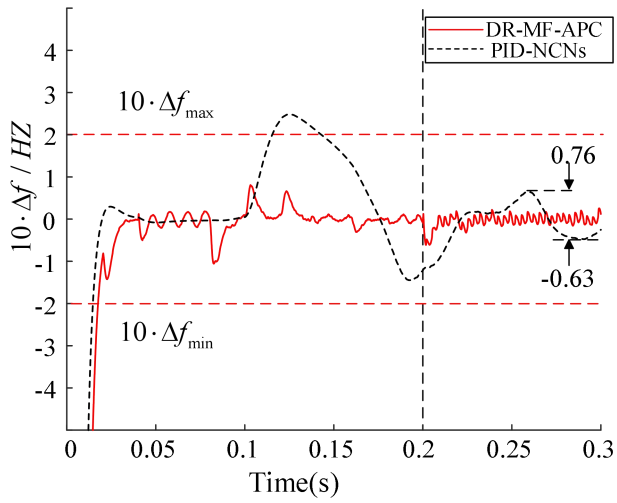

Fig. 6. System frequency fluctuation

The harmonic analysis of the bus voltage was conducted for the time intervals 0–0.12s, 0.08–0.22s, and 0.18–0.3s. The results of this analysis are presented in Fig.6. A comparison of the performance between the negative sequence compensation recovery strategy and the DR-MF-APC active recovery strategy is illustrated in Fig.7(a) and 7(b).

In Fig.7, 'Mag' represents the ratio of harmonic to fundamental amplitude, while 'THD' denotes the total harmonic distortion rate. The harmonics generated by asymmetrical loads and DG self-grouping before 0.2s are

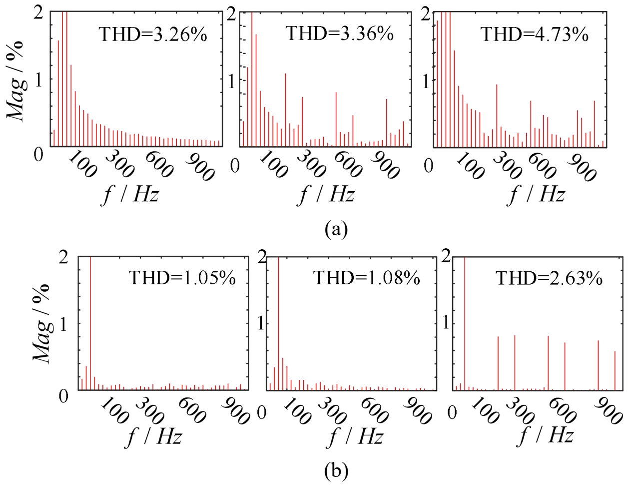

Fig. 7. Bus voltage harmonics
(a, negative sequence compensation strategy b, DR-MF-APC decentralized control strategy)

primarily low-order harmonics. After 0.2s, when nonlinear loads are connected to the grid, the harmonics are predominantly odd-order, with harmonic amplitudes decreasing as frequency increases.

When the operating conditions of the AC-MG change, the DR-MF-APC active recovery strategy iteratively updates its parameters based on collected data, significantly reducing the harmonic content of the bus voltage compared to the negative sequence compensation recovery strategy. While the negative sequence compensation recovery strategy results in higher bus voltage harmonic content when compensating for negative sequence voltage drops, the DR-MF-APC strategy exhibits a superior suppression effect on low-frequency harmonics compared to its performance before the improvement.

C. Control law weight factor variation system performance

The decentralized controllers consisting of data-driven MF-APC and DR-MF-APC have a similar structure and both contain λ . When the only online parameter to be regulated, λ changes, the individual DG outputs will adjust accordingly. In this case, the selection of different λ values can be considered as a parameter perturbation for controlling bus voltage and frequency. To assess the robustness of the proposed control strategy to parameter perturbations, simulations are designed. The parameters are provided in Tables II and III.

The simulation results are compared at λ with 8.3 and 16.6, respectively. As shown in Figure 8, MF-APC is more sensitive to the selection of λ , and the, with the frequency change exceeding the specified range. Additionally, the time required to reach steady state is longer compared to the improved DR-MF-APC, indicating that the sensitivity of the DR-MF-APC to the selection of the MF-APC is reduced.

In practical applications, the weighting factor λ can control the input variation, the. The smaller λ is, the faster the transient response of the system; however, this may lead to a larger steady-state frequency error or even system instability. Conversely, a larger results in a slower transient response but a smaller steady-state frequency error. Therefore, selecting the optimal parameter requires careful consideration of the specific application scenario.

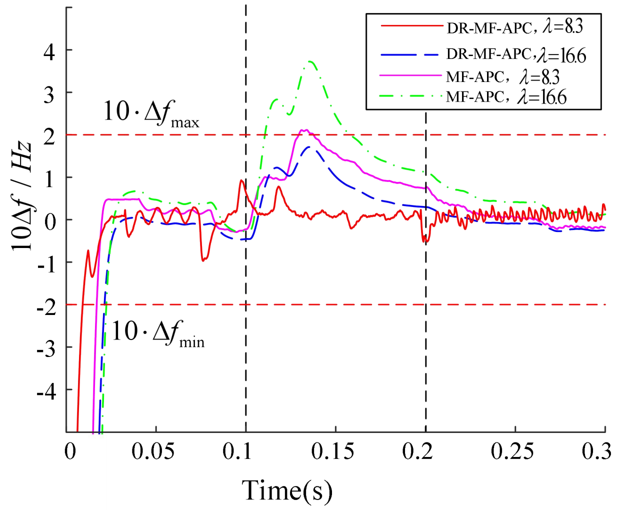

Fig. 8. System frequency error under different data-driven control strategies

As shown in Fig.9, under different control strategy parameters, the MF-APC, with the same data-driven algorithm before the change of λ , demonstrates a good suppression effect on network fluctuations for both general load groups and unbalanced load groups (3 and 9). The voltage amplitude fluctuation is similar to that of the DR-MF-APC, with the amplitude error stabilized at 0.3 and the voltage imbalance degree stabilized at 0.003. However, the suppression effect of the MF-APC on the transient process of the DG's self-organization network during the active restoration process is not satisfactory. The reason for this is that variations in the weighting factor λ across different controllers result in differences in output power quality, which, in turn, impact the power grid.

As the value of λ changes, the amplitude of bus voltage and unbalanced oscillation changes significantly. Specifically, the amplitude error before and after the change in DR-MF-APC voltage amplitude increases from 0.6 to 0.7, and the unbalance degree increases from 0.004 to 0.02. In contrast, the amplitude error before and after the change in MF-APC voltage amplitude increases from 1.1 to 1.5, and the unbalance degree increases from 0.003 to 0.03. It can be seen that for AC-MG with a short-time time-varying structure, DR-MF-APC can improve the safety stability of active recovery to some extent. As shown in TABLE IV, Comparison with MF-APC method in literature [24].

TABLE IV
COMPARISON WITH MF-APC METHOD

λ	Index	MF-APC	DR-MF-APC
$\lambda=8.3$	Frequency error(max)	2.1Hz	0.8Hz
	Voltageamplitude error	1.1	0.6
	Unbalance degree	0.03	0.02
$\lambda=16.6$	Frequency error	3.8Hz	1.7Hz
	Voltageamplitude error	1.5	0.7
	Unbalance degree	0.003	0.004

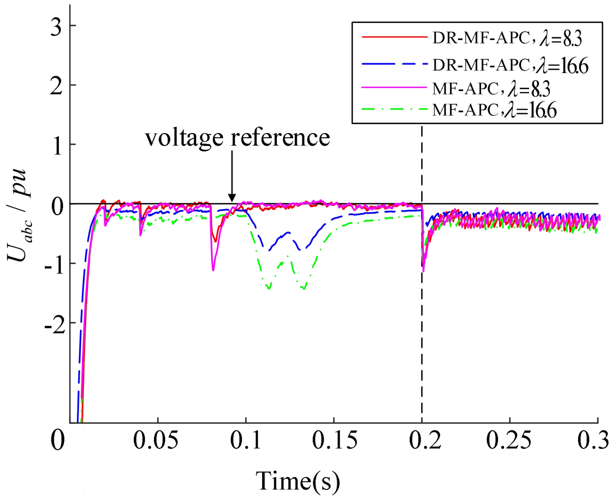

(a)

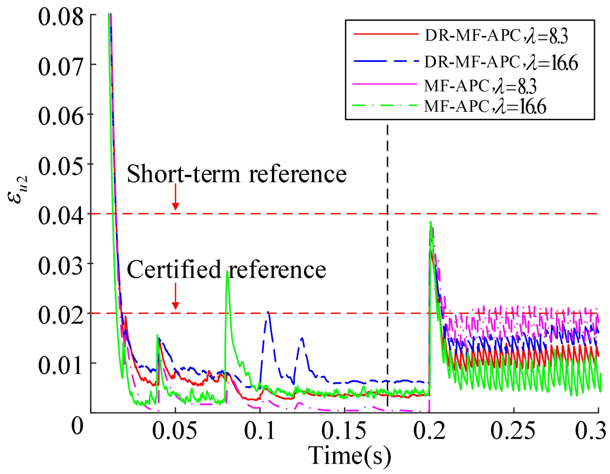

(b)

Fig. 9. Bus voltage unbalance fluctuation under different data-driven strategies
(a, bus voltage magnitude; b, bus voltage unbalance)

VI. Conclusion

In this paper, a data-driven decentralized controller is designed based on the local power information of DGs under no-communication conditions to address voltage/frequency fluctuations and high harmonic content caused by nonlinear asymmetric loads, which are difficult to suppress by the system droop control during the active recovery of islanded AC-MG. This controller functions as a secondary controller, which helps maintain the system frequency and voltage close to their nominal values with minimal error. At the same time, it suppresses the bus voltage imbalance and harmonics generated by the system.

The MF-APC and DR-MF-APC methods were compared and analyzed while taking λ as 8.3 and 16.6. The imbalance of the DR-MF-APC increased from 0.004 to 0.02, while the imbalance of the MF-APC increased from 0.003 to 0.03. The sensitivity of the controller's key parameter λ selection was found to be further reduced with the DR-MF-APC method.

Simulation results of the islanded microgrid indicate that the designed decentralized controller can ensure the voltage/frequency stability of the AC-MG active recovery system. Since this paper focuses on the algorithm, it does not consider the effects of noise and interference in the input and output data. Therefore, future work will involve incorporating bad data detection and filtering mechanisms for practical applications. Additionally, we will consider the trade-off between control accuracy and the large volume of calculation data, which may cause challenges in data storage. Future studies will also explore the influence of noise and interference in input/output data on the system and extend the algorithm to active recovery of microgrid cyber-physical systems (CPS) under network attack.

References

[1] H. Chen, Z. Tang, J. Lu. "Optimal scheduling of microgrids based on CVAR quantitative uncertainty," Power System Protection and Control, vol. 49, no. 5, 2018, pp. 105-115.

[2] Chao-Hong B, Chao-Fan L, Geng-Feng L, Ai-Ci Q. "Development and prospect of flexible power system under energy transition," Chinese Journal of Electrical Engineering, vol. 40, no. 9, 2020， pp. 2735-2745.

[3] X. Gu, Y. Bai, S. Li. "A review of research on black-start recovery in power systems," Journal of Electro-technology, vol. 37, no. 13, 2022, pp. 3183-3200.

[4] J. Li, H. Yu, C. Li. "Black-start power coordination strategy for wind-solar storage based on model predictive control," Grid Technology, vol. 44, no. 10, 2020, pp. 3700-3708.

[5] W. Liu, Y. Liu. "Hierarchical model predictive control of wind farm with an energy storage system for frequency regulation during black-start," International Journal of Electrical Power & Energy Systems, 2020, 119: 105893.

[6] N. Xie, P. H. Yang, P. He. "Research on energy storage control strategy for the whole process of the black start of thermal power units in the wind and solar storage microgrid," Journal of Power System and Automation, vol. 35, no. 2, 2023, pp. 75-82.

[7] C. Chen, J. Gao, Y. Cao. "Smoothing of voltage/frequency fluctuations during active islanding recovery in multi-source distribution networks," Journal of Shanghai Jiao Tong University, vol. 56, no. 5, 2022, pp. 543.

[8] Zhu Y, Zhou Y, Wang Z, Zhou C, Gao B. "A terminal distribution network black-start optimization method based on pruning algorithm considering distributed generators," Energy Reports, 2022, 8: 237-244.

[9] Y. Shi, X. Yang, J. Su. "Control strategy for unbalanced voltage compensation in microgrid system," Power system automation, vol. 41, no. 23, 2017, pp. 96-102.

[10] J. Lai, T. Xie, J. H. Su. "Coordinated control of voltage unbalance compensation for islanded microgrid based on particle swarm optimization algorithm," Power System Automation, vol. 44, no.16, 2020, pp. 121-129.

[11] Q. Cheng, P. Ye, L. Wei. "Input power control of TLDMC based on sliding mode control under grid imbalance conditions," High Voltage Technology, vol. 47, no.12, 2021,pp. 11.

[12] Z. Lan, R. Hao, H. Jiu. "Optimal foresight control of three-phase inverter based on repetitive control and state feedback ," Journal of Electro-technology, vol. 37, no.6, 2022, pp. 1473-1481.

[13] H. Lhachimi, Y. Sayouti, Y. Kouari. "Control of a flexible microgrid during both modes of operations with the presence of nonlinear loads," Journal of the Franklin Institute, vol.357, no.11, 2020, pp. 6498-6538.

[14] L. Zhang, X. Li, W. Zhang. "Optimization-based restoration strategy for microgrids considering multi-objective criteria," IEEE Transactions on Smart Grid, vol.15, no.2, 2024, pp.1225-1236.

[15] J. Liu, S. Wang, M. Chen. "A deep learning approach for self-healing in microgrids," Renewable Energy, vol.184, 2024, pp.344-355.

[16] H. Wu, Y. Zhang, Z. Guo. "Distributed energy management for fast recovery of microgrids after faults," Applied Energy, vol.325, 2024, pp.118458.

[17] T. Chen, Z. Yu, P. Huang. "Real-time data analysis for fault detection and microgrid restoration using IoT," International Journal of Electrical Power & Energy Systems, vol.142,2024,pp. 107672.

[18] X. Zhao, F. Sun, Y. Li. "Communication-assisted coordination strategy for microgrid restoration," IEEE Access, vol.12, 2024, pp. 87976-87987.

[19] X. Zhang, M. Liu. "Fault-tolerant control strategies for microgrid restoration in islanded mode," Journal of Energy Storage, vol.45, 2024, pp. 103429.

[20] Zhang H, Zhou J, Sun Q, Guerrero J. M, Ma D. "Data-driven control for interlinked AC/DC microgrids via model-free adaptive control and dual-droop control," IEEE Transactions on Smart Grid, vol.8, no.2, 2015, pp. 557-571.

[21] Zhang S, Zhou P, Xie Y, Chai T. "Improved model-free adaptive predictive control method for direct data-driven control of a wastewater treatment process with high performance," Journal of Process Control, 2022, 110: 11-23.
[22] Wang S, Li J, Hou Z, Meng Q, Li M. "Composite Model-free Adaptive Predictive Control for Wind Power Generation Based on Full Wind Speed," CSEE Journal of Power and Energy Systems, vol.8, no.6, 2020, pp. 1659-1669.
[23] Hu C, Yin Z, Rui T, Zhang Z, Shen W, Cao W, Holmes D. G. "An improved model-free predictive control method for voltage source inverters," Power Electronics Technology, vol.56, no.6, 2022, pp. 53-56.
[24] Cheng L, Wu W, Qiu L, Liu X, Ma J, Zhang J, Fang Y. "An improved data-driven based model predictive control for zero-sequence circulating current suppression in paralleled converters," International Journal of Electrical Power & Energy Systems, 2022, 143: 108401.
[25] Y. Mi, J. Chang, S. Shi. "Data-driven secondary control of islanded DC microgrid," Power Automation Equipment, vol.41, no.5, 2021, pp. 7.
[26] Z. Hou, S. Jin. "Model-free adaptive control: theory and applications," Science Press, 2013, pp.124-130.
[27] Bu X, Yu Q, Hou Z, Qian W. "Model-free adaptive iterative learning consensus tracking control for a class of nonlinear multiagent systems," IEEE Transactions on Systems, Man, and Cybernetics: Systems, vol.49, no.4, 2017, pp. 677-686.
[28] X. Wu, M. Wang, X. Shi. "Additional damping control method for sub-synchronous oscillation of doubly-fed wind turbine based on model-free adaptive control," Chinese Journal of Electrical Engineering, 2022(042-010).

Tengfei Wei (M.S. '13–Ph.D. '20) received his M.S. degree in 2013 and his Ph.D. degree in 2020. He is currently an associate professor at the School of Electrical and Information Engineering, Lanzhou University of Technology. His research interests include intelligent control and information processing, instrumentation and automation equipment, power electronics, smart microgrid systems, distributed power systems, photovoltaic power generation control technology, and applications of ARM and FPGA.
XueFeng Zhang(M.S. candidate '22–Present) has been pursuing a master's degree at Lanzhou University of Technology in Lanzhou, China, since 2022. His research focuses on smart microgrid systems and distributed energy.
LiXin Wang(M.S. '22) graduated from Lanzhou University of Technology in Lanzhou, China. He is currently employed at Ningxia Electric Power Company, China, where his research focuses on microgrid network security control.